ISSN: 2476-6909; Modares Mechanical Engineering. 2024;24(10):611-619.

# Evolution of The Conventional Rotary Forging Machines to Six-DoF Parallel Kinematics Machines

**ARTICLE INFO**

***Article Type***
Original Research

***Authors***
Zarhoon A.[1],
Nategh M. J.[1*],
Manafi D.[1],

**How to cite this article**
Zarhoon A, Nategh M.J, Manafi D, Evolution of The Conventional Rotary Forging Machines to Six-DoF Parallel Kinematics Machines. Modares Mechanical Engineering; *2024;24(10):611-619.*

**ABSTRACT**

Rotary forging is an incremental bulk forming process, possessing salient advantages compared with the conventional forging, including reduced force, smoothness of operation, lower investment, apt for near net shaping and producing workpieces with intricate profiles. However, the conventional rotary forging machines suffer serious limitation in their kinematics, which originates from their simple eccentric mechanism of the actuating device. The parallel-kinematics hexapod mechanism with six degrees of freedom can circumvent this limitation. The theory and practice of this concept has been successfully implemented in the present study. The inverse kinematics of hexapod has been adapted to the kinematics of the rotary forging processes. This could yield a proper method to generate the orbitally rocking motion prevailing in the process. In order to investigate the material flow in the lower die, physical modeling was carried out by the use of plasticine and several experiments were conducted in a hexapod machine. The final shapes of the workpieces, the degrees of die filling, and the forging forces were compared with the conventional forging, indicating improved results. It was observed that the motion pattern in the rotary forging influences the time and the force required for forming. The maximum forces required for rotary forging using the circular and planetary motion patterns were 32 N and 38 N respectively. In comparison, conventional forging required a significantly higher force, approximately 200 N. The time required to form a bevel gear using planetary motion was almost half of the time needed for circular motion.

**Keywords** Rotary Forging, Obital Forging, Rocking Die, Hexapod, Stewart Platform, Parallel Kinematics.

[1] Mechanical Engineering Department, Tarbiat Modares University, Tehran, Iran.

***Correspondence***
Address: Mechanical Engineering Department, Tarbiat Modares University, Tehran, Iran.

nategh@modares.ac.ir

***Article History***
Received: September 15, 2024
Accepted: December 16, 2024
ePublished: December 29, 2024

**CITATION LINKS**

1- Investigation of Motion Profiles of Forming Tool in .... 2- Processing design and optimization on rotary forging of .... 3- Comparison between cold rotary forging and conventional forging. 4- Orbital forming of flange parts under uncertainty. 5- Mechanical properties of .... 6- A review of force reduction methods in .... 7- Comparative analysis of classical forging and orbital forging of .... 8- A Feasibility Study on Performing Rotary Forging Process by Hexapod Table and Estimation of .... 9- Reconfiguration and tool path planning of .... 10- Development of rotary forging machines: from idea to .... 11- An investigation into the rotary foging process capabilities and .... 12- Orbital cold forming technology-combining high quality forming with .... 13- Upper-bound analysis of the rotary forging of .... 14- Calculating force and energy during rotating forging. 15- The influence of technological parameters on .... 16- Explanation of the mushroom effect in the rotary forging of .... 17- Effect of size of the cylindrical workpiece on .... 18- 3D FE modeling simulation of .... 19- On the specifics of modelling of .... 20- Cold orbital forging of gear rack. 21- Rotary forging with .... 22- Research on forming technology of rotary forging with .... 23- Grain Refinement Mechanism of .... 24- Microstructure and mechanical property evolution mechanisms .... 25- Modeling for warping prediction and control in .... 26- Modeling for plastic instability in multi-directional rotary forging of .... 27- Efficiently manufacturing large-scale isotropic Al7075 alloy sheets with submicron grain by .... 28- Influence of rotary forging and post-deformation annealing on mechanical and .... 29- An investigation into forming of .... 30- Flexible forming with hexapods. 31- Control of integrated electro-hydraulic servo-drives in .... 32- The kinematic modeling and simulation of an .... 33- Robot modeling and control. 34- Plastometric tests for plasticine as ....

## 1- Introduction

In rotary forging, two dies are employed, one of which (lower die) accommodates the billet. The end of the other die (upper die) is conical with its axis situated in the vertical plane. This axis is inclined from the vertical axis of the lower die with a small angle (usually from 2 to 10 degrees). This angle leads to applying forging force only on a small surface of the workpiece. This is the reason for reduction of the forming force that has been reported to be between $\frac{1}{5}$ to $\frac{1}{10}$ of the conventional forging[1,2]. The upper die orbitally moves on the surface of the workpiece inside the lower die, and the lower die moves upward under a constant feedrate. The forming region continuously develops inside the workpiece, and the shaping is gradually done until the final form is obtained.[3,4] The efficiency of this process is usually high, and the waste is little. The forged parts have better mechanical properties[5]. The rotary forging is generally slow for hot forging mass production; however, it is feasible for automatic cold forging. This method is used for near net shaping[6]. However, in the common rotary forging machines, the limitation of the die movement is a serious deficiency limiting the wider application of this process[7]. The second author of this paper suggested hexapod machine to replace the conventional rotary forging machine. This concept has already been realized[8], but is still in its embryonic phase. The parallel mechanism in the hexapod machine allows for high stiffness, low mass, agility, and high acceleration, making it suitable for high-speed processing[9].

The technical capabilities of the conventional machines are determined by their kinematic designs, which are very different[10]. Nategh and Mehdinejad[11] designed and made a rotary forging machine with adjustable motor rotation to achieve different motion patterns. Sivam et al.[12] conducted a brief study on the properties of rotary forging and compared it with conventional method. Choi et al.[13] addressed the analysis of rotary forging with the upper-bound theorem and found out that with the increase in the inclination angle of the upper die from 1 to 4 degrees, a significant force reduction is obtained. They found that the forming force is also reduced with the decrease in the feed rate. Zhang[14], using the upper-bound analysis method, calculated the force and energy needed during the rotary forging. Rusz and Dyja[15] addressed the effects of parameters such as the inclination angle of the upper die, the die rotation speed, and the size and form of the workpiece in the rotary forging. Liu et al.[16], proposed a 3-dimensional limited element method for simulation of the rotary forging process to reveal the workpiece's deformation and investigate the mushroom effect. They found out that if the height-to-diameter ratio of the billet is in the range of 0.5-1, the mushroom effect would occur.

L. Hua and X. Han[17] investigated the effects of a cylindrical workpiece's dimensions on the rotary forging process. It was illustrated that with the increase in the initial radius of the cylindrical workpiece, less mushroom effect was observed in the deformed workpiece, and the deformation became more uniform, while the maximum shaping force and torque were gradually increased. With the increase in the initial height of the cylindrical workpiece, the mushroom effect becomes more evident in the deformed piece, and the deformation becomes more non-uniform. At the same time, the maximum shaping force and torque are gradually increased. L. Hua and X. Han[18] found that with an increase in the feed rate, the mushroom effect decreased. Krishnamurthy et al.[19] modeled the rotary forging process by using Metal Forming Simulation Software (Qform). Han et al.[20] developed a method of cold rotary forging for manufacturing a gear rack under straight line motion pattern. Liu et al.[21] addressed the manufacture of very thin disks with large diameters using rotary forging. R. F. Ma et al.[22] investigated the rotary forging process to form large-diameter disks with double symmetry rolls. They concluded that when the feed rate is higher than its allowable limit, eccentric defect and warping occur. If the rolling speed is very high or the coefficient of friction between the tapered roll and the workpiece is much lower than the coefficient of friction between the lower die and the workpiece, the workpiece would undergo center thinning or even rupture.

Producing complex sheet components using conventional forming processes, such as stamping and forging, poses significant challenges. Cold rotary forging, however, stands out as an ideal method for fabricating intricate sheet components due to its ability to enable continuous and localized plastic deformation of the metal. Cold rotary forging holds immense potential for manufacturing sheet parts with sophisticated geometries. Despite this promise, comprehensive studies on the mechanisms driving microstructural evolution during cold rotary forging remain limited, restricting its application in producing components with precisely controlled geometries and microstructures. In this context, Xinghui Han et al.[23] investigated the mechanisms of grain refinement in 5A06 aluminum alloy sheets during cold rotary forging. Xinghui Han et al.[24] conducted an in-depth study on the microstructure and the mechanisms underlying the evolution of mechanical properties in aviation gear steel during the cold rotary forging process. Cold rotary forging is particularly suitable for forming circular plates due to its continuous localized plastic deformation characteristics. However, the process often encounters warping defects during the forging of circular plates. These issues arise from the eccentric load applied by the conical upper die, which can lead to poor forming accuracy and even material waste. Yaxiong Hu et al.[25] developed a predictive and control model for warping in cold rotary forging of circular plates. The model calculates the extent of warping and reveals that increasing the feed per revolution or decreasing the tilt angle of the upper die exacerbates the warping defect. To address this, they proposed a novel warping control method by adjusting the offset distance of the rotational center of the upper die, offering a practical solution to enhance the precision of cold rotary forging for circular plates.

Multi-directional rotary forging (MRF) is a localized plastic forming process characterized by its low forging force. MRF is widely used in the production of bevel gears, flanges, and other complex components. Due to its technical advantages and broad application prospects for efficiently manufacturing

high-performance complex parts, extensive research has been conducted on MRF. With its incremental deformation nature and smaller forging loads, MRF demonstrates significant potential for shaping thin-walled components. However, for thin-walled parts with thick ribs, plastic instability is more likely to occur at the base of the ribs during MRF, leading to waste and defects in the components. The stress-strain state and metal flow in MRF are complex, which can result in certain forming defects. Yaxiong Hu et al.[26] developed a model to predict plastic instability in multi-directional rotary forging of thin-walled components with three ribs.

Typically, metal sheets are produced through a unidirectional rolling process, which tends to create a strong single-crystal texture. This inevitably induces significant anisotropy. Anisotropy in rolled sheets severely compromises their post-forming capabilities. Xuan Hu et al.[27] utilized the MRF process to adjust the isotropy degree and grain structure of Al7075 sheets. Andreev et al.[28] investigated the effects of thermomechanical processing regimes, including hot rotary forging and post-deformation annealing at various temperatures and holding times, on the structure and mechanical properties of a TiNi alloy. The study revealed that rotary forging results in the formation of an ultrafine-grained structure in the TiNi alloy, characterized by a high density of defects and refined structural elements. Abd-Eltwab et al.[29] proposed a novel method for forming gears and threaded parts using a new rotary forging tool. They demonstrated that forming speed, die dimensions, and tool diameter significantly influence die filling and the forming load.

The parallel mechanism has been recently considered for the forming purposes, by some researchers. Hesselbach et al.[30] have used a hydraulically actuated hexapod as a flexible forming tool and managed to develop a hydraulically controlled hexapod. Hosseini and Nategh[8] investigated the feasibility of implementing the rotary forging process by servomotor-actuated hexapod machine. They concluded that hydraulically actuated hexapod with the proper hydraulic control can do the purpose. Wos and Dindrof[31] addressed the parallel mechanism's kinematics, dynamics, and control for the forging process. The force and position control with compatible controllers were analyzed in this mechanism. They verified that multiaxial electro-hydraulic control architecture allows for high precision and multi-electrohydraulic synchronization.

The combinational theory of the kinematics of rotary forging process and hexapod tool needs to be developed by taking the pivot point into consideration. This has been undertaken by the present authors. This theory paves the way for creating different, theoretically limitless, motion patterns for implementing rotary forging process by the use of hexapod machines. Several experiments were carried out to manufacture plasticine bevel gear to verify the theory and to ensure the efficacy of the process. The results were compared with conventional forging.

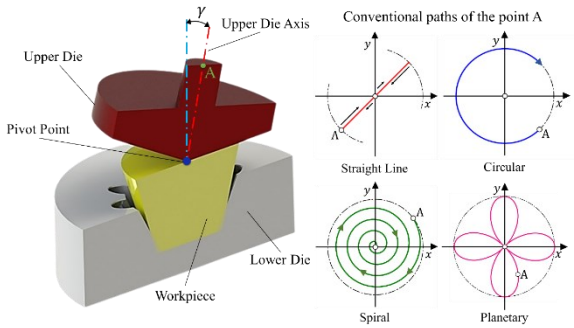


**Fig. 1)** Configuration of the conventional rotary forging process and prevalent motion patterns.

## 2- Rotary forging with hexapod machine

### 2-1- Introduction to the dominant parameters in rotary forging

A schematic view of rotary forging is illustrated in Fig. 1. During the rotary forging process with the conventional machines, the lower die moves upward with a constant speed of $v$ until the workpiece reaches the final height. In the rotary forging, the contact area between the upper die and the workpiece is a portion of an Archimedean spiral. When the lower die stops its axial feed movement, the upper die should still revolve around the machine's axis for few more revolutions until the upper surface of the workpiece becomes flat and smooth.

In order to produce sound parts in the rotary forging, a specified and predetermined pattern and motion path for the upper die during the process is required. This motion path significantly influences the material flow inside the lower die, and the force needed for the forming process. The selection of a proper motion pattern is, therefore, very important. In conventional machines, the motion patterns are created by the rocking movement of the upper die (Fig. 1). In this figure, the configuration of the upper and the lower dies, their relative motion, the rocking motion of the upper die around the fixed pivot point, and the motion profiles commonly produced by the conventional rotary forging machines are illustrated. The linear, circular, spiral, and planetary profiles of the upper die's motion paths are depicted in the Fig. 1. Some other profiles can also be produced on the basis of these basic shapes. However, they are very limited and cannot be suitably adapted to various forging shapes.

### 2-2- Rotary forging by hexapod machine and the relevant parameters

The configuration of implementing the rotary forging process in the hexapod machine is shown in Fig. 2. The hexapod mechanism possesses two platforms; one is stationary (not shown in Fig. 2), and the other is movable. The moving platform carries the lower die. These platforms are connected to each other by six pods through spherical and universal joints, providing six degrees of freedom. Three pods are shown in Fig. 2. Each pod is, in fact, a sliding actuator, which is extended or contracted by using a servomotor or a hydraulic actuator. The velocity and acceleration of the axial extension and contraction of each pod is independently controlled. The combined effect of these linear motion results in any motion profile of the moving platform.

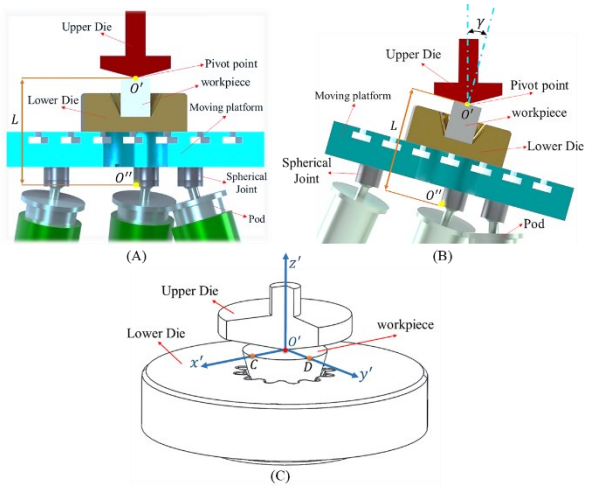


**Fig. 2)** ((A) And (B))-the configuration of the hexapod rotary forging machine, (C)-workpiece contacting with the upper die at the pivot point.

When the hexapod is employed as a rotary forging machine, the lower die accommodating the billet is fastened centrally to the moving platform. The motion profile is applied to the lower die through the moving platform, contrary to the conventional machines where the upper dies undergo the required motion profiles. The upper die is fixed in a vertical spindle and remains vertically stationary in contact with the billet inside the lower die (Fig. 2-A). The feed motion is a part of the total motion of the lower die defined along the three Cartesian axes and around them. By controlling the $o-xyz$ coordinates of the moving platform's center point and platform's orientation around these axes, the motion profile and the feed movement of the lower die is controlled at each instance through the inverse kinematics. The motion profile and the feed movement of the lower die are, thus, directly defined by the lengths of pods which are governed by the inverse kinematics. Theoretically, there is no limit for the total motion of the lower die in hexapod machine except for those induced because of the physical limits of the machine within its workspace. The moving platform and, thus, the lower die move and assume different poses within the hexapod's workspace. An example pose of the upper platform together with the lower die, at an arbitrary point of the hexapod's workspace is shown in Fig. 2-B. The local coordinate system attached to the upper platform at its virtual center point, and the coordinate system attached to the top surface of workpiece at the pivot point are illustrated in Fig. 2-C. The rocking motion and the feed motion that are commonly applied to the upper die and the lower die, respectively, in the conventional rotary forging process, are all embodied in the motion of the hexapod's end effecter. As can be evidenced in Fig. 2, these two kinds of motion are not differentiated from each other. Both are imparted by the servo controller through an inverse kinematics core computer program, in the form of linear and rotational motion of the end effecter along and around the three Cartesian coordinate's axes.

In Fig. 3, $u_i$ and $s_i$ show the locations of universal and spherical joint centers, respectively, and $\boldsymbol{l}_i$ shows the length vector of the legs, ( $i=1,2,\dots,6$ ). The $o''-x''y''z''$ coordinates system is attached to the moving platform with

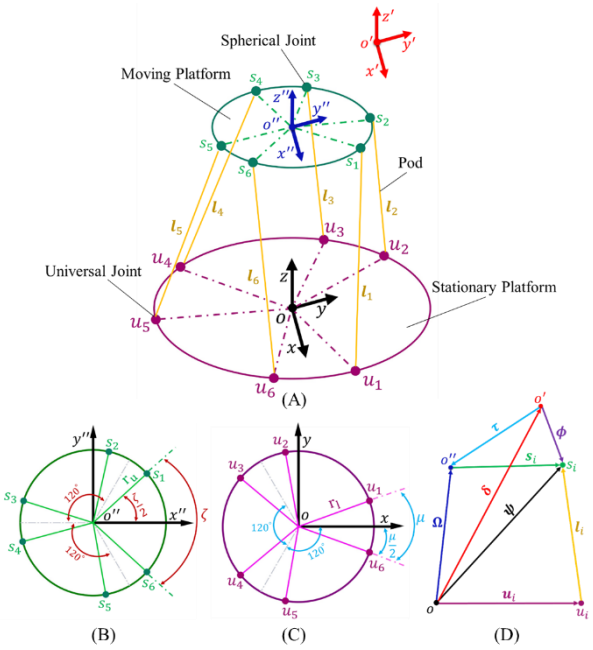


**Fig. 3)** (A)-Schematic of the hexapod mechanism with coordinate systems, (B)-locations of spherical joints on the moving platform, (C)-locations of spherical joints on the stationary platform, (D)-inverse kinematic chain for a leg.

**Table 1)** Structural parameters of the hexapod.

| Parameters | $r_u\ (mm)$ | $r_l\ (mm)$ | $\zeta\ (rad)$ | $\mu\ (rad)$ |
|---|---|---|---|---|
| Values | 125 | 325 | 1.483 | **0.698** |

its origin at the center of the platform, the $z''$ axis perpendicular to the upward moving platform, and the $x''$ axis perpendicular to the imaginary line $s_1s_6$. The $o-xyz$ coordinates system is attached to the center of the stationary platform, with its $z$ axis perpendicular to the stationary platform, and its $x$ axis perpendicular to the imaginary line $u_1u_6$. In Fig. 3, $r_l$ and $r_u$ are the radii of the stationary and moving platform, respectively, and $\zeta$ and $\mu$ are the angular distances between the spherical joints and universal joints, respectively.

The matrix $\boldsymbol{S}$, which includes the vectors of the locations of the spherical joints $(\boldsymbol{s}_i \mid i=1,2,\dots,6)$ in the $o''-x''y''z''$ coordinate system (Fig. 3) is obtained, as follows:

$$S=[s_1 \quad s_2 \quad s_3 \quad s_4 \quad s_5 \quad s_6]$$

$$=\begin{bmatrix} (r_u)\cos(\frac{\zeta}{2}) & (r_u)\cos(\frac{2\pi}{3}-\frac{\zeta}{2}) & -(r_u)\cos(\frac{\pi}{3}-\frac{\zeta}{2}) & -(r_u)\cos(\frac{\pi}{3}-\frac{\zeta}{2}) & (r_u)\cos(\frac{2\pi}{3}-\frac{\zeta}{2}) & (r_u)\cos(\frac{\zeta}{2}) \\ (r_u)\sin(\frac{\zeta}{2}) & (r_u)\sin(\frac{2\pi}{3}-\frac{\zeta}{2}) & (r_u)\sin(\frac{\pi}{3}-\frac{\zeta}{2}) & -(r_u)\sin(\frac{\pi}{3}-\frac{\zeta}{2}) & -(r_u)\sin(\frac{2\pi}{3}-\frac{\zeta}{2}) & -(r_u)\sin(\frac{\zeta}{2}) \\ 0 & 0 & 0 & 0 & 0 & 0 \end{bmatrix} \quad (3)$$

The matrix $\boldsymbol{U}$, which includes the vectors of the locations of the universal joints $(\boldsymbol{u}_i \mid i=1,2,\dots,6)$ in the $o-xyz$ coordinate system (Fig. 3) is obtained, as follows:

$$U=[u_1 \quad u_2 \quad u_3 \quad u_4 \quad u_5 \quad u_6]$$

$$=\begin{bmatrix} (r_l)\cos(\frac{\mu}{2}) & -(r_l)\sin(\frac{\pi}{6}-\frac{\mu}{2}) & -(r_l)\sin(\frac{\pi}{6}+\frac{\mu}{2}) & -(r_l)\cos(\frac{\pi}{3}-\frac{\mu}{2}) & -(r_l)\cos(\frac{\pi}{3}+\frac{\mu}{2}) & (r_l)\cos(\frac{\mu}{2}) \\ (r_l)\sin(\frac{\mu}{2}) & (r_l)\cos(\frac{\pi}{6}-\frac{\mu}{2}) & (r_l)\cos(\frac{\pi}{6}+\frac{\mu}{2}) & -(r_l)\sin(\frac{\pi}{3}-\frac{\mu}{2}) & -(r_l)\sin(\frac{\pi}{3}+\frac{\mu}{2}) & -(r_l)\sin(\frac{\mu}{2}) \\ 0 & 0 & 0 & 0 & 0 & 0 \end{bmatrix} \quad (4)$$

The structural parameters of the 6-dof hexapod are presented in Table 1:

### 2-3- Kinematics of rotary forging hexapod machine

As mentioned earlier in this paper, the pivot point corresponding with the contact point between the upper die and the top surface of the workpiece at any deformation instant (Fig. 2), remains stationary at the same position. The hexapod controller determines the position of the plate passing through the centers of the spherical joints by changing the lengths of the legs. The center of this plate is named the center of the hexapod's moving platform ($o''$) (Fig. 3). On the other hand, the motion path in the rotary forging is planned based on the pivot point. Therefore, the relationship between the lengths of the legs and the pivot point should be determined so that the new controller specifically designed for the hexapod rotary forging machine can determine the lengths of the legs at each instant, by using the inverse kinematics.

The $o-xyz$ , $o''-x''y''z''$ , and $o'-x'y'z'$ coordinate systems are denoted by the frame 1 ($\mathcal{F}_1$), frame 2 ($\mathcal{F}_2$), and frame 3 ($\mathcal{F}_3$), respectively. The pivot point $o'$ is represented in the coordinate system $o'-x'y'z'$ (Fig. 3).

For the kinematic chain in Fig. 3-D, $\psi$ is the location vector of the spherical joint in coordinates frame 1, $\delta$ is the location vector of the arbitrary pivot point in coordinates frame 1, $\Omega$ is the location vector of the the center of moving platform in coordinates frame 1, $\tau$ is the location vector of the center of the moving platform in coordinates frame 3, and $\phi$ is the location vector of the spherical joint in coordinates frame 3. The location of the desired pivot point can be expressed in the global coordinates system ($o-xyz$) and its orientation can be represented by the relative orientation of $\mathcal{F}_1$ and $\mathcal{F}_3$.

$$\delta = [x_{o'} \quad y_{o'} \quad z_{o'}]^T \tag{5}$$

The rotation matrix is defined, as follows (relative orientation of $\mathcal{F}_1$ and $\mathcal{F}_2$:

$$\boldsymbol{R} = \begin{bmatrix} C(\beta).C(\gamma) & -C(\beta).S(\gamma) & S(\beta) \\ (S(\alpha).S(\beta).C(\gamma)) + (C(\alpha).S(\gamma)) & -(S(\alpha).S(\beta).S(\gamma)) + (C(\alpha).C(\gamma)) & -S(\alpha).C(\beta) \\ -(C(\alpha).S(\beta).C(\gamma)) + (S(\alpha).S(\gamma)) & (C(\alpha).S(\beta).S(\gamma)) + (S(\alpha).C(\gamma)) & C(\alpha).C(\beta) \end{bmatrix} \tag{6}$$

Where symbols $S$ and $C$ represent $Sin$ and $Cos$, respectively.

The upward feed component of the platform's motion is relatively small and, therefore, the top surface of the workpiece can be approximately considered as a plane during the process. This plane is parallel to the hypothetical plane passing through the center of the spherical joints. In other words, the orientation of these two planes relative to the global coordinate system $o-xyz$ are the same.

The following transformation relation exists for any arbitrary vector $\boldsymbol{\rho}$ [32]:

$$^2\rho + \tau = {}^3\rho \tag{7}$$

The position of $o''$ in the $o'-x'y'z'$ coordinates system is defined as follows:

$$\tau = [x_{o'o''} \quad y_{o'o''} \quad z_{o'o''}]^T \tag{8}$$

The location vector of $i$-th spherical joint in the $o'-x'y'z'$ coordinates system is defined as follows:

$$\phi = s_i + \tau \tag{9}$$

The location vector of $i$-th spherical joint in the $o-xyz$ coordinates system can be expressed as follows (Fig. 3-D):

$$\psi = R.\phi + \delta \tag{10}$$

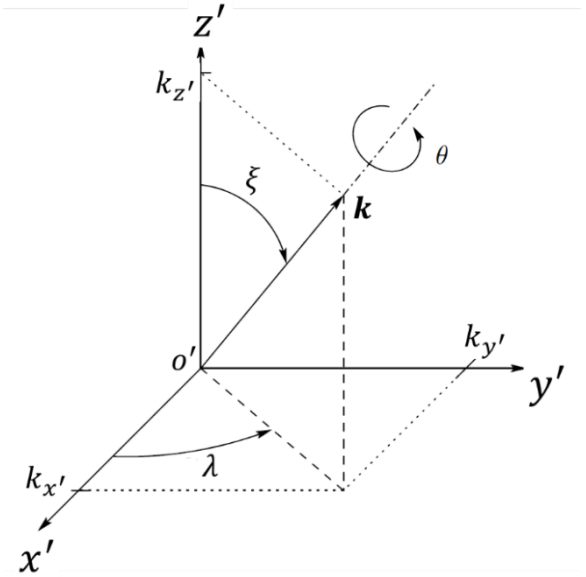


**Fig. 4)** Rotation around an arbitrary axis.

With the aid of inverse kinematics, the length vector of the $i$-th leg (Fig. 3-D) is:

$$l_i = \psi - u_i = R.\phi + \delta - u_i \tag{11}$$

The length the $i$-th leg is obtained, as follows:

$$l_i = |l_i| = \sqrt{(l_i)^T.(l_i)} = \sqrt{(R.\phi + \delta - u_i)^T.(R.\phi + \delta - u_i)} \tag{12}$$

The rotation is not always performed around the main axes in $o'-x'y'z'$ coordinates system. For some motion patterns, such as the planetary and circular motion, the rotation around an arbitrary axis in space is required (Fig. 4).

If the rotation axis is an arbitrary vector $\boldsymbol{k}$ (Fig. 4), the equivalent rotation matrix is obtained, as follows [33]:

$$R(k,\theta) = \begin{bmatrix} k_{x'}^2(1-C(\theta)) + C(\theta) & k_{x'}k_{y'}(1-C(\theta)) - k_{z'}S(\theta) & k_{x'}k_{z'}(1-C(\theta)) + k_{y'}S(\theta) \\ k_{x'}k_{y'}(1-C(\theta)) + k_{z'}S(\theta) & k_{y'}^2(1-C(\theta)) + C(\theta) & k_{y'}k_{z'}(1-C(\theta)) - k_{x'}S(\theta) \\ k_{x'}k_{z'}(1-C(\theta)) - k_{y'}S(\theta) & k_{y'}k_{z'}(1-C(\theta)) + k_{x'}S(\theta) & k_{z'}^2(1-C(\theta)) + C(\theta) \end{bmatrix} \tag{13}$$

Where symbols $S$ and $C$ represent $Sin$ and $Cos$, respectively. When the rotation around the main axes is not expressed in the local coordinates, the matrix $\boldsymbol{R}(\boldsymbol{k},\theta)$ replaces the matrix $R$. By knowing the position of the pivot point, the controller determines the lengths of the legs (Eq. 12), through inverse kinematics.

### 2-4- Proposed method

In order to shape a forging in hexapod, a suitable pattern needs to be defined for the motion of the lower die. The motion pattern is obtained from the combination of the rotation (rocking) of the lower die around the pivot point and feeding in the $z$ direction. The motion pattern should conform to the shape of the lower die and the final forging. It directly influences the contact area between the upper die and the workpiece, and has a significant role in filling the lower die cavity. In general, the first step in the rotary forging process is to ensure the alignment of the workpiece, and the lower and upper dies. The moving platform together with the lower die installed on it is, then, actuated to move upward until the billet inside the lower die contacts the upper die at the pivot point. The geometrically predefined pattern is, then,

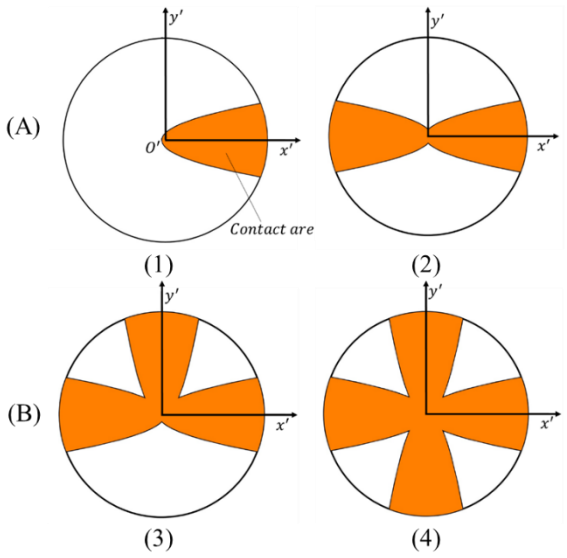


**Fig. 5)** Creation of contact areas with the implementation of two perpendicular straight-lines motion pattern.

applied to the moving platform by actuating the legs through the inverse kinematics control.

For all the considered motion patterns, the feed motion in $z$ direction is applied at each step. The straight-line is the simplest motion pattern in rotary forging, and it is implemented in the hexapod by rocking the lower die around an axis passing from the pivot point. After the establishment of the contact point between the workpiece and the upper die at the pivot point, the lower die is tilted by the maximum inclination angle of the upper die (γ) around an axis passing through the center of rotation (for example, $y'$ in Fig. 2-C) until the workpiece touches the upper die along a line. Then the feed motion is applied in the $z$ direction and the contact area is formed from the intersection of the upper die and the upper surface of the workpiece (Fig. 5-A). The rocking motion then takes place around the same axis on the other side of the lower die. Rocking around the next axis is done according to the desired movement pattern (the motion pattern of two perpendicular straight-lines (Fig. 5-B)) and this cycle continues until the final forging is obtained.

The circular motion pattern consists of rocking around several axes passing through the pivot point (several straight-lines) (Fig. 6-A).

The planetary motion pattern consists of rotation around two perpendicular axes passing through the pivot point, so that after rocking in one direction around the first axis (for example, $y'$ in Fig. 2-C) and establishment of contact between the preform and the upper die at the pivot point, the lower die implements its feed motion in the $z$ direction. The rocking takes place in both directions of the secondary axis ($x'$ in Fig. 2-C) which is perpendicular to the first axis, so that point $D$ and a similar point on the other side come into contact with the upper die. This action is repeated in the other direction of the first axis ($y'$) and by changing the first and secondary axis and repeating the described steps, a planetary contact surface is formed between the upper die and the workpiece (Fig. 6-B).

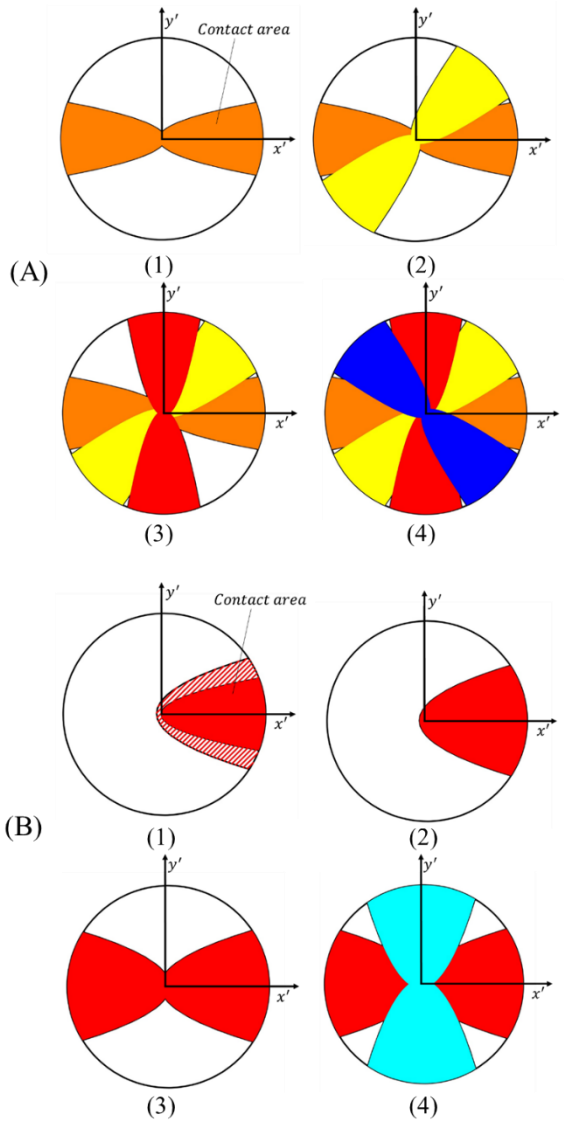


**Fig. 6)** (A)-creation of contact areas with the implementation of a circular motion pattern, (B)-creation of contact areas with the implementation of a planetary motion pattern.

## 3- Experiments

A bevel gear was produced in a setup consisting of a hexapod moving platform for carrying the lower die and imparting the required motion profiles to it, and a milling machine the spindle of which carried the upper die and imparted the required positing movement to this die. All experiments have been done by using plasticine as the test material.

It should be noted that plasticine is very sensitive to strain rate and its deformation behavior is very complex[34].

Each test was repeated in four iterations. The proposed method was followed to create smooth movement for the flow of material and filling of the lower die. The motion path of the center of the moving platform was planned by a specially developed inverse kinematics program and imparted through six servomotors to the pods' actuators. In addition, the bevel gear was also produced by the conventional forging, and the force needed for the conventional forging was compared to that of the rotary forging.

### 3-1- Experimental setup

The forming machine used in the current study was the hexapod machine tool available in the "Advanced Technologies in Machine Tools" (ATMT) laboratory, equipped with servo actuators (Fig. 7). The upper die was made of mild steel with a conic angle of 3 degrees, and with a maximum diameter of 70 mm (Fig. 7). The geometry of the lower die cavity matched the final forging shape.

Unlike paraffin wax, plasticine is not self-lubricating. Therefore, friction on the contact surfaces should be reduced by using oil. Lubricant will be used to remove the plasticine from the lower die more easily. A lubricant solution of SAE 40 oil together with light polyethylene (nylon) was used during the process.

Since the deformation force of plasticine is low, it can easily be displaced and undergo unwanted movement inside the lower die, resulting in undesirable shaping. In order to prevent this, the plasticine billet needs to be preformed to match the die cavity. The raw material is, therefore, shaped close to the die cavity with a very simple preform die.

Fused Deposition Modeling (FDM) is an additive manufacturing method that allows for the production of the parts from the 3-D model and with the desired geometrical shape without the need to preparing any tool. The preform die made of PLA (Polylactic Acid) material was produced with this method (Fig. 8). To produce the bevel gear with the conventional forging, the universal SANTAM tension and compression machine was used. A Kistler dynamometer model 9257BA was used to measure the required force of rotary forging. The accuracy of this three dimensional dynamometer is ±1 N. The experimental conditions are shown in Table 2.

**Table 2.)** Process parameters adopted in experiment.

| Parameters | Values |
|---|---|
| Initial maximum diameter of preform (mm) | **44.5** |
| Initial height of preform (mm) | **30** |
| Height reduction ($\frac{\Delta h}{h_0}$ %) (mm) | **33.33** |
| Inclination angle of the upper die (°) | **3** |

### 3-2- Test results

The resultant of the three components of the forging load measured by the dynamometer is considered as the rotary forging force. The bevel gear was formed by the use of the proposed method. Different motion profiles were tested for the lower die, for the purpose of testing the influence of these profiles on the sound production of the bevel gear. These included two perpendicular straight lines, circular and planetary motion patterns. It was expected that the more matching between the movement path and the workpiece geometry, the better are the material flow and die filling. It was, actually, observed the filling of the bevel gear die was much better by the circular and planetary motion patterns. The maximum force required for rotary forging in the circular motion pattern (32 N) was lower than that of planetary motion (38 N) (Fig. 9). The maximum force in the conventional forging was approximately 200 N.

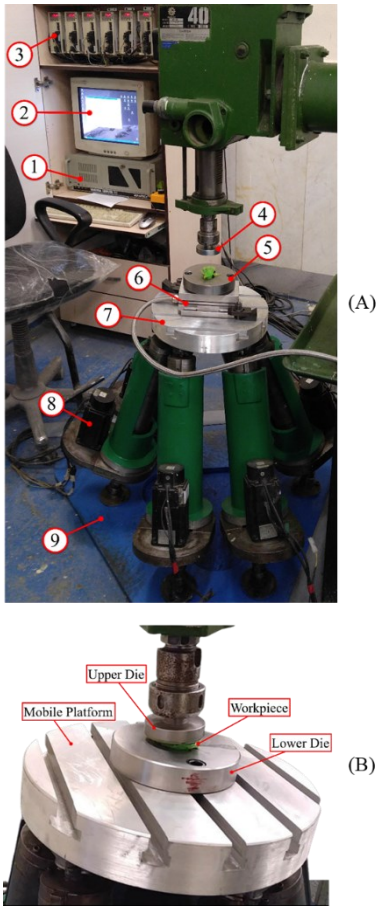


**Fig. 7)** (A) Experimental setup with dynamometer; 1-Industrial computer, 2-Hexapod motion controller, 3-Servo controller, 4-Upper die, 5-Lower die, 6-Dynamometer, 7-Mobile platform, 8-Servo motor, 9- Stationary platform. (B) Experimental setup before installing the dynamometer.

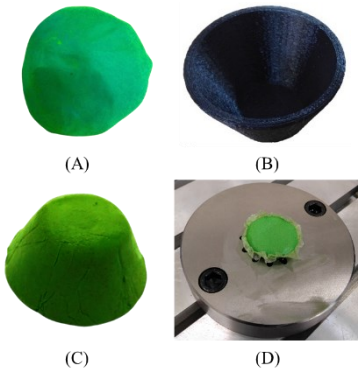


**Fig. 8)** Preparation of plasticine preform for rotary forging, (A)-primary raw material, (B)-preform die made of PLA, (C)-preform, (D)-locating the preform with lubricant inside the lower die.

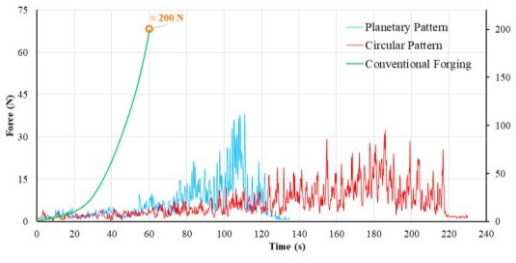


**Fig. 9)** Force-Time graph for rotary forging of bevel gear by the use of planetary and circular motion patterns.

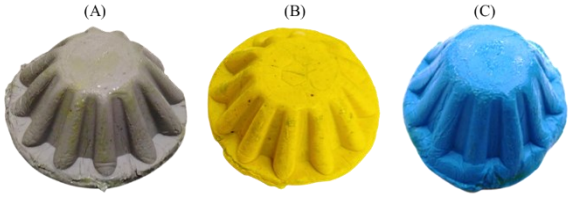


**Fig. 10)** The test results with the proposed method for forging the bevel gear, (A)-with circular motion pattern, (B)-with planetary motion pattern, and (C)-with two perpendicular straight-lines motion pattern.

## 4- Results and discussion

It was observed that rotary forging was viable by using a hexapod machine. The best results for the production of the bevel gear was obtained by the use of planetary and circular motion patterns, compared with linear motion (Fig. 10). The ratio of the maximum force in the rotary forging to the conventional forging was about 0.2. The force started from a minimum value and ended at a maximum value due to the change in the contact area (Fig. 9). The increase in force occurred due to the increase of the upper die's penetration depth into the billet. After the feed movement was complete, the rocking motion continued for at least two more cycles so that the upper surface of the workpiece could become flat and smooth. Therefore, the amount of force during the experiments reduced after reaching its maximum value at the end of the forming process. The motion pattern in the rotary forging influenced the process time (Fig. 9). The time needed to form bevel gear by planetary motion was nearly half (0.587) the time required to form the gear by circular motion. The maximum force required for forming with circular motion was lower than that needed with planetary motion. The ratio of forming force for bevel gear with circular motion to the force with planetary motion was 0.84.

Plasticine is very sensitive to the change of strain rate and its deformation behavior is complex. Different colors of plastic are obtained by adding different factors to a base material. This means that the overall composition of each color is different from other colors. Therefore, one can expect changes in the mechanical behavior of plastic from one color to another. The deformation force varies among plasticines with different colors available in the market. A motion pattern closer to the final shape was expected to have a better result (in terms of force and deformation time). However, this could not be exactly verified as the sensitivity of plasticine caused problems and errors in the results. Any additional movement between the upper die and plasticine, such as attachment and detachment, resulted in the unwanted displacement of billet. In future research, for a better investigation, lead or steel should be used for experiments in order to be able to comment on the effect of different motion patterns on lower die filling.

## 5- Conclusion

The conventional machines used in rotary forging have kinematic limitations in producing the path of die motion for complicated parts. With six degrees of freedom, the hexapod mechanism allows for the rotary forging of complex parts. This device can produce theoretically unlimited motion patterns for any forging geometry. In the current study, the relationship between the position of the pivot point and the legs' lengths has been obtained for smooth paths along straight lines, and planetary or circular patterns. It has been illustrated that the rotary forging can successfully be implemented with a hexapod machine. In order to investigate the material flow in the lower die and compare the forging force in rotary forging with its counterpart in the traditional process, several experiments have been carried out by the use of plasticine. It was observed that the best results for the production of a bevel gear was obtained by the use of planetary and circular motion patterns, compared with linear motion. The exact conformity between the profile of forging and the die's motion pattern could not be verified by the model material, as the latter was quite sensitive to any extra movement between the upper die and the plasticine. The authors expect that this would be verified with industrial materials in their future work. The maximum force needed for the rotary forging was about 0.2 of that needed in the conventional forging of the bevel gear. It was also observed that the motion pattern in the rotary forging influences the time and the force required for forming.

## Nomenclature:

| | |
|---|---|
| $^{A}\boldsymbol{p}$ | Expression of vector $\boldsymbol{p}$ in coordinates frame of $A$ |
| $\mathcal{F}_1$ | Coordinates frame of the hexapod's stationary platform |
| $\mathcal{F}_2$ | Coordinates frame of the hexapod's moving platform |
| $\mathcal{F}_3$ | Coordinates frame of the pivot point |
| $h_0$ | Initial height of preform (mm) |
| $h_c$ | Initial height of center thinning (mm) |
| $r_l$ | Radius of stationary platform (mm) |
| $r_u$ | Radius of moving platform (mm) |
| $H_0$ | Initial height of the workpiece (mm) |
| $S_{min}$ | Minimum feed rate (mm/rev) |
| $l_i$ | Magnitude of the $i$-th leg's length vector; |
| $o'$ | Pivot point |
| $o'-x'y'z'(\mathcal{F}_3)$ | Coordinates system attached to the workpiece at the pivot point |
| $o''$ | Center of hexapod's moving platform |
| $r_w$ | Radius of workpiece (mm) |
| $s_i$ | Location of the $i$-th spherical joint |
| $u_i$ | Location of the $i$-th universal joint |
| $\boldsymbol{l}_i$ | The $i$-th leg's length vector |
| $h$ | Final height of the workpiece (mm) |
| $L$ | Distance between the hypothetical and parallel Planes passing through the pivot point and the Center of the spherical joints (mm) |
| $S$ | Feed rate (mm/rev) |
| $n$ | Rotational speed of the upper die (rev/s) |
| $o$ | Center of hexapod's stationary platform |
| $o''-x''y''z''\ (\mathcal{F}_2)$ | Coordinates system attached to the moving platform |
| $o-xyz\ (\mathcal{F}_1)$ | Global coordinate system |
| $t$ | Forming time (s) |
| $v$ | Axial feed rate (mm/s) |
| $\boldsymbol{R}$ | First rotation matrix |
| $\boldsymbol{R}(\boldsymbol{k},\theta)$ | The rotation matrix around the arbitrary axis $\boldsymbol{k}$, under the angle $\theta$ degrees |
| $\gamma$ | Inclination angle of the upper die |
| $\zeta$ | Angular distance between spherical joints |
| $\mu$ | Angular distance between universal joints |

## Ethical Statement

The content of this manuscript is original, based on the authors' research, and has not been published or submitted elsewhere, either in Iranian or international journals.

## Conflict of interest

The authors declared that they have no conflicts of interest to this work.

## References

1- Kherad G, Nategh MJ, Ghazawi MR. Investigation of Motion Profiles of Forming Tool in Orbital Forging Process. Proc 4th Conf Manufacturing Engineering,; Feb. 15-16; Tehran: Amir Kabir University of Technology; 1999. p. 176-84.
2- Gu B, Han X, Hua L. Processing design and optimization on rotary forging of thin-walled structure. Thin-Walled Structures. 2021;162:107567.
3- Han X, Hua L. Comparison between cold rotary forging and conventional forging. Journal of mechanical science and technology. 2009 Oct;23:2668-78.
4- Calmano S, Hesse D, Hoppe F, Traidl P, Sinz J, Groche P. Orbital forming of flange parts under uncertainty. Applied Mechanics and Materials. 2015 Dec 13;807:121-9.
5- Kovářík O, Čech J, Čapek J, Hajíček M, Klečka J, Siegl J. Mechanical properties of forged tungsten heavy alloys.
6- Politis DJ, Politis NJ, Lin J, Dean TA. A review of force reduction methods in precision forging axisymmetric shapes. The International Journal of Advanced Manufacturing Technology. 2018 Jul;97:2809-33.
7- Plančak M, Kačmarčik I, Stefanović M, Skakun P, Vilotić D. Comparative analysis of classical forging and orbital forging of cross joint component. Advanced Technologies and Materials. 2015 Dec 21;40(2):43-54.
8- Hosseini SV, Nategh MJ. A Feasibility Study on Performing Rotary Forging Process by Hexapod Table and Estimation of Forming Load for a Cylindrical Workpiece. Modares Mechanical Engineering. 2016 Aug 10;16(6):41-51.
9- Li Z. Reconfiguration and tool path planning of hexapod machine tools. New Jersey Institute of Technology; 2000. 10- Aksenov LB, Kunkin SN. Development of rotary forging machines: from idea to additive technologies. Sciences of Europe. 2016(7-2 (7)):4-11.
11- Nategh M. An investigation into the rotary foging process capabilities and load estimation. (No Title). 1995:417-24.
12- Sivam SSS, Sekar VU, Mishra A, Mondal A, Mishra S. Orbital cold forming technology-combining high quality forming with cost effectiveness-A review. Indian Journal of Science and Technology. 2016;9(38).
13- Choi S, Na KH, Kim JH. Upper-bound analysis of the rotary forging of a cylindrical billet. Journal of Materials Processing Technology. 1997 May 1;67(1-3):78-82.
14- Zhang M. Calculating force and energy during rotating forging. In3 rd International Conference on Rotary Metalworking Processes(ROMP 3) 1984 (pp. 115-124).
15- Rusz S, Dyja H. The influence of technological parameters on the rotary pressing process. Journal of materials processing technology. 2004 Dec 20;157:604-8.
16- Liu G, Yuan SJ, Wang ZR, Zhou DC. Explanation of the mushroom effect in the rotary forging of a cylinder. Journal of materials processing technology. 2004 Sep 1;151(1-3):178-82.
17- Han X, Hua L. Effect of size of the cylindrical workpiece on the cold rotary-forging process. Materials & Design. 2009 Sep 1;30(8):2802-12.
18- Hua L, Han X. 3D FE modeling simulation of cold rotary forging of a cylinder workpiece. Materials & Design. 2009 Jun 1;30(6):2133-42.
19- Krishnamurthy B, Bylya O, Muir L, Conway A, Blackwell P. On the specifics of modelling of rotary forging processes. Computer Methods in Materials Science. 2017 Jan 15;17(1):22-9.
20- Han X, Hu Y, Hua L. Cold orbital forging of gear rack. International Journal of Mechanical Sciences. 2016 Oct 1;117:227-42.
21- Liu X, Zhu C, Sun S, Ma R. Rotary forging with multi-cone rolls. Journal of Manufacturing Processes. 2020 Aug 1;56:656-66.
22- Ma RF, Zhu CD, Gao YF, Wei ZH. Research on forming technology of rotary forging with double symmetry rolls of large diameter: thickness ratio discs. Mechanical Sciences. 2021 Jun 10;12(1):625-38.
23- Han X, Chen W, Hu X, Hua L, Chai F. Grain Refinement Mechanism of 5A06 Aluminum Alloy Sheets during Cold Rotary Forging. Materials. 2023 Mar 29;16(7):2754.
24- Han X, Chen L, Hu X, Hua L, Chai F. Microstructure and mechanical property evolution mechanisms of 15Cr14Co12Mo5Ni2WA aviation gear steel during cold rotary forging. Journal of Materials Research and Technology. 2023 May 1;24:3005-22.
25- Hu Y, Han X, Hua L, Zhuang W. Modeling for warping prediction and control in cold rotary forging of round plate. Journal of Materials Processing Technology. 2023 Apr 1;313:117865.
26- Hu Y, Han X, Hua L, Zhuang W. Modeling for plastic instability in multi-directional rotary forging of thin-walled components with three ribs. Journal of Materials Processing Technology. 2024 Oct 1;331:118522.
27- Hu X, Han X, Chai F, Zhuang W, Zheng F, Yin F, Xie L, Hua L. Efficiently manufacturing large-scale isotropic Al7075 alloy sheets with submicron grain by multidirectional rotary forging. Materials & Design. 2024 Feb 1;238:112713.
28- Andreev VA, Karelin RD, Komarov VS, Cherkasov VV, Dormidontov NA, Laisheva NV, Yusupov VS. Influence of rotary forging and post-deformation annealing on mechanical and functional properties of titanium nickelide. Metallurgist. 2024 Jun 4:1-8.
29- Abd-Eltwab AA, Elsyed Ayoub W, El-Sheikh MN, Saied EK, Ghazaly NM, Gomaa AA. An investigation into forming of gears using rotary forging process. Manufacturing Technology. 2024 Sep 1;24(4):539-51.
30- Hesselbach J, Behrens BA, Dietrich F, Rathmann S, Poelmeyer J. Flexible forming with hexapods. Production Engineering. 2007 Dec;1:429-36.
31- Dindorf R, Wos P. Control of integrated electro-hydraulic servo-drives in a translational parallel manipulator. Journal of Mechanical Science and Technology. 2019 Nov;33:5437-48.
32- Tan S, Liang F, Chen L, Lin Z. The kinematic modeling and simulation of an adjustable pivot point of Six Degree-Of-Freedom (DOF) Parallel Robot. InJournal of Physics: Conference Series 2021 (Vol. 1739, No. 1, p. 012034). IOP Publishing.
33- Spong MW, Hutchinson S, Vidyasagar M. Robot modeling and control. John Wiley & Sons; 2020 Mar 30.
34- Wójcik Ł, Lis K, Pater Z. Plastometric tests for plasticine as physical modelling material. Open Engineering. 2016 Dec 30;6(1).